iScience

CellPress
OPEN ACCESS

Article

Prion-derived tetrapeptide stabilizes thermolabile insulin via conformational trapping

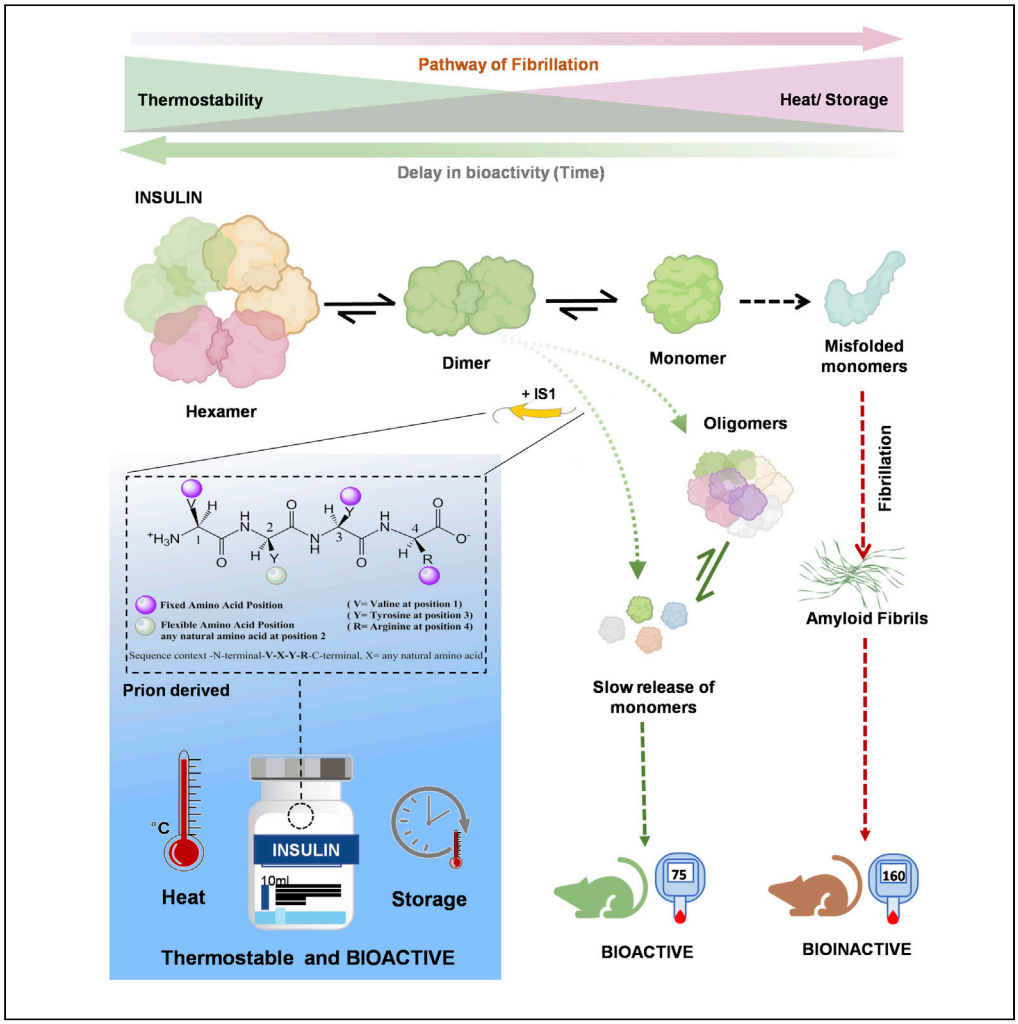

Meghomukta Mukherjee, Debajyoti Das, Jit Sarkar, ..., Samit Chattopadhyay, Subhrangsu Chatterjee, Partha Chakrabarti

subhro_c@jcbose.ac.in, subhrangsu@gmail.com (S.C.)
pchakrabarti@iicb.res.in (P.C.)

Highlights

Prion-derived consensus tetrapeptide motif V(X)YR protracts insulin fibrillation

IS1 (VYYR) preserves bioactive insulin under varying physicochemical perturbations

IS1 serves as nontoxic, cell-impermeable peptide excipient for insulin

IS1 conformationally traps dimeric insulin during fibrillation

Mukherjee et al., iScience 24, 102573
June 25, 2021
https://doi.org/10.1016/j.isci.2021.102573

iScience

CellPress
OPEN ACCESS

Article

Prion-derived tetrapeptide stabilizes thermolabile insulin via conformational trapping

Meghomukta Mukherjee,[1,6] Debajyoti Das,[2,6] Jit Sarkar,[2,3,7] Nilanjan Banerjee,[1,7] Jagannath Jana,[1] Jyotsna Bhat,[1] Jithender Reddy G,[4] Jagadeesh Bharatam,[4] Samit Chattopadhyay,[5] Subhrangsu Chatterjee,[1,*] and Partha Chakrabarti[2,3,8,*]

SUMMARY

Unfolding followed by fibrillation of insulin even in the presence of various excipients grappled with restricted clinical application. Thus, there is an unmet need for better thermostable, nontoxic molecules to preserve bioactive insulin under varying physiochemical perturbations. In search of cross-amyloid inhibitors, prion-derived tetrapeptide library screening reveals a consensus V(X)YR motif for potential inhibition of insulin fibrillation. A tetrapeptide VYYR, isosequential to the β2-strand of prion, effectively suppresses heat- and storage-induced insulin fibrillation and maintains insulin in a thermostable bioactive form conferring adequate glycemic control in mouse models of diabetes and impedes insulin amyloidoma formation. Besides elucidating the critical insulin-IS1 interaction (R4 of IS1 to the N24 insulin B-chain) by nuclear magnetic resonance spectroscopy, we further demonstrated non-canonical dimer-mediated conformational trapping mechanism for insulin stabilization. In this study, structural characterization and preclinical validation introduce a class of tetrapeptide toward developing thermostable therapeutically relevant insulin formulations.

INTRODUCTION

Availability of injectable insulin formulation has been a breakthrough in diabetes management in achieving long-term glycemic control and preventing complications (Baram et al., 2018; Heller et al., 2007; Moroder and Musiol, 2017; Owens et al., 2001; Xiong et al., 2019; Zaykov et al., 2016); it still, however, suffers from certain disadvantages including temperature-sensitive fibrillation in solution and development of subcutaneous tumor-like mass designated as "amyloidoma" at the site of injection (Hua and Weiss, 2004; Ivanova et al., 2009; Nilsson, 2016; Woods et al., 2012; Yumlu et al., 2009). Worldwide efforts were thus made to develop thermostable insulin either by making recombinant insulin species with mutations or stabilizing native insulin with salts, Zn^{2+} ions, and small molecules such as meta-cresol (Frankær et al., 2017; Gong et al., 2014; Han et al., 2017; Kachooei et al., 2014; Lee et al., 2014; Patel et al., 2018; Saithong et al., 2018; Wang et al., 2011; Zheng and Lazo, 2018). However, small molecules are found to be toxic in long-term usage and are inefficient in optimally preventing fibrillation (Teska et al., 2014; Weber et al., 2015). Thus, the unmet need for better nontoxic insulin stabilizers is highly warranted and nonimmunogenic peptides as stabilizers would have no or very low toxicity (Banerjee et al., 2013; Neddenriep et al., 2012; Wu, 2019). To date, an array of peptide-based stabilizers was designed and validated through *in silico* or biophysical investigations, but the exploration of their therapeutic potential in *in vitro*, *in cellulo*, and *in vivo* preclinical models is mostly lacking (Das and Bhattacharyya, 2017; Mishra et al., 2013; Ratha et al., 2016; Seidler et al., 2018; Wallin et al., 2018). Recent advances suggest screening and designing of cross-amyloid inhibitors can either protracts amyloid self-assembly or inhibit potential cross-seeding of interacting amyloidogenic proteins (Armiento et al., 2020).

In the search for endogenous peptide motifs that could potentially hinder insulin fibrillation and stabilize insulin in its stable conformation, we looked at misfolded human prion conformers because of its colocalization at insulin-secreting pancreatic β-cells while having a converse functional association with glucose homeostasis (Amselgruber et al., 2006; Ashok and Singh, 2018). Three conserved tetrapeptide motifs (RYYR/VYYR/AYY(D/Q)) found in PrPc and the conformation-selective surface exposure of "YYR" associated with the β-sheet structure in misfolded PrP^{Sc} prompted us to consider these peptide motifs as the

[1]Department of Biophysics, Bose Institute, Kolkata, India

[2]Division of Cell Biology and Physiology, CSIR-Indian Institute of Chemical Biology, 4 Raja SC Mullick Road, Kolkata 700032, India

[3]Academy of Innovative and Scientific Research, Ghaziabad 201002, India

[4]Centre for NMR and Structural Chemistry, CSIR-Indian Institute of Chemical Technology, Uppal Road, Tarnaka, Hyderabad, India

[5]Division of Cancer Biology & Inflammatory Disorder, CSIR-Indian Institute of Chemical Biology, Kolkata, India

[6]These author contributed equally

[7]These author contributed equally

[8]Lead contact

*Correspondence: subhro_c@jcbose.ac.in, subhrangsu@gmail.com (S.C.), pchakrabarti@iicb.res.in (P.C.)

https://doi.org/10.1016/j.isci.2021.102573

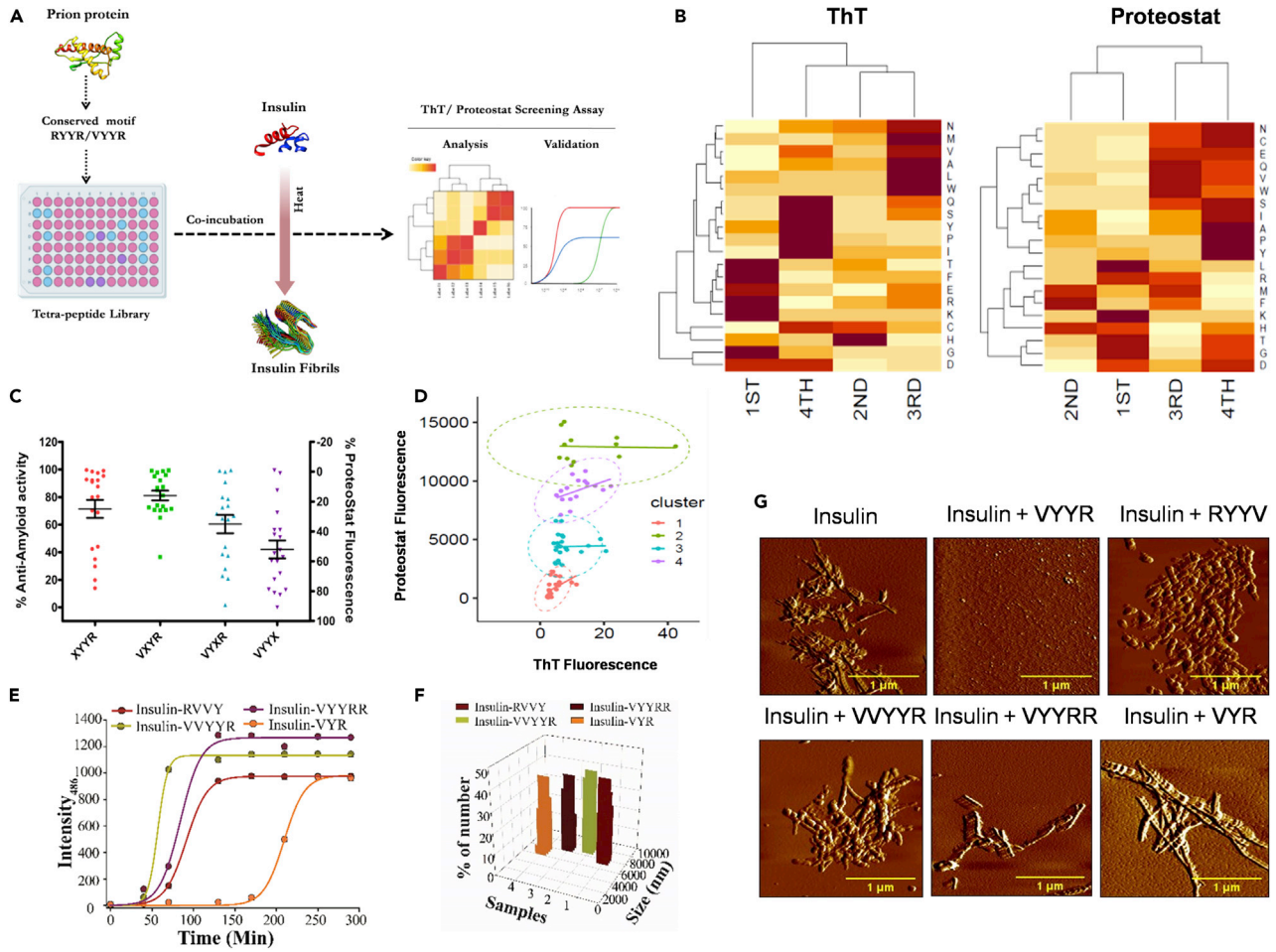

Figure 1. Prion-derived peptide screening for antiamyloid activity

(A) Schematic representation of antiamyloid peptide screening.

(B) Heatmap of hierarchical clustering of fibrillated insulin in the presence of equimolar ratio of 77 tetrapeptide variants. Darker shades represent higher fluorescence values.

(C) Amyloid activity as an inversely proportional function of PROTEOSTAT fluorescence distributed in 4 tetrapeptide sequence.

(D) Four independent clusters of peptides obtained from k-means clustering.

(E and F) ThT assay and DLS for heat-induced fibrillation of insulin in the presence of indicated peptides.

(G) AFM for heat-induced fibrillation of insulin (scale bars, 1 μm).

seeding platform to design cross-amyloid inhibitors for insulin amyloidosis (Julien et al., 2009; Paramithiotis et al., 2003).

RESULTS

Peptide screening reveals insulin stabilizing prion-derived tetrapeptide sequence

We designed a library of 77 tetrapeptides based on two conserved tetrapeptide motifs (RYYR/VYYR), each having a single amino acid substitution at a time by the rest 19 natural amino acids for each position (Table S1). Peptides were screened for the heat-induced insulin fibrillation inhibition using thioflavin T (ThT) and PROTEOSTAT fluorescence (Figure 1A; S1A, $r = 0.59, p \leq 0.001$). Heatmap of fluorescence data revealed that peptides having the formula of V-(X)-Y-R have the highest antiamyloid potential (~81.4%), whereas V-Y-Y-(X) peptides showed the lowest impact (44.24% inhibition), where X is any amino acid (Figures 1B and 1C). Even unsupervised K-means clustering showed that cluster-1 containing 27 peptides had the lowest fluorescence values (5.5% of native insulin) and highest antiamyloid potential (Figure S1C) with significant correlation ($R = 0.46$, $p = 0.017$) (Figure 1D). Cluster-1 peptides were further analyzed for percent allowable substitution [(substitution observed/total possible substitution i.e. 19) * 100] at each position that depicts

marked conservation of amino acids at the third and fourth positions by allowing only 21.05% and 15.5% substitutions, respectively, making the Y(3)-R(4) sequence indispensable for the anti-fibrillating property. We thereby propose a generalized tetrapeptide sequence V-(X)-Y-R that would potently prevent insulin fibrillation.

To test the position-dependent importance of the core Y-Y sequence, we used five peptides (V-Y-Y-R, V-P-P-R, V-Y-P-R, V-P-Y-R, and V-T-T-R) for heat-induced insulin fibrillation assay. Only V-Y-Y-R showed significant antiamyloid activity and preserved insulin's glucose-lowering capacity during an insulin tolerance test (ITT) in mice (Figures S2A–S2D). We further designed variant peptides by adding amino acid at N- and C-terminal of VYYR (VVYYR and VYYRR), deleting one tyrosine from the core sequence (VYR) and reversing the sequence to RYYV. VVYYR, VYYRR, and RVVY did not inhibit insulin fibrillation as confirmed by atomic force microscopy (AFM) studies and corroborating these results with corresponding ThT and dynamic light scattering (DLS) data, whereas VYR showed modest inhibitory effects than the rest of the peptide variants as depicted by the ThT assay (Figures 1E–1G). Altogether, these results prompted us to select V-Y-Y-R (now termed IS1) as a candidate for insulin stabilization and further validate its therapeutic potential in preclinical mice models and commercial insulin formulations.

IS1 protects insulin from both heat- and storage-induced fibrillation

The kinetics of heat-induced insulin fibrillation with varying molar ratios of insulin:IS1 by revealing dose-dependent inhibition insulin fibrillation maximally at the equimolar concentration is shown by ThT fluorescence and AFM (Figure 2A). The interaction of insulin and IS1 determined by isothermal titration calorimetry (ITC) by fitting the titration curve in the one-site binding model (Figure S3A) was thermodynamically favorable ($\Delta G = -4.8$ kcal.mol^{-1}, $\Delta H = -18.73$kcal.mol^{-1}, $\Delta S = -46.5$ kcal.mol^{-1}; $K_A = 3.46 \times 10^{-3}M^{-1}$). IS1 remarkably restored the hydrodynamic radius of insulin monomers, otherwise which was increased to 1000 nm at 150 min of heating (Figure 2B). Circular dichroism (CD) spectroscopy showed gradually decay in dual negative ellipticities at 208 nm and 222 nm, which indicates the loss of α-helical conformation for native insulin owing to heat-induced fibrillation, whereas the presence of IS1 retained its conformations even after 5 h (Figure 2C and Table S2). To test its therapeutic relevance, we have tested its antiamyloid potential in commercial human insulin formulation (Actrapid) both in the presence and absence of commercial excipients for heat-induced and storage-induced (37°C, 30 days) fibrillation. AFM data showed that IS1 inhibits Actrapid fibrillation by trapping insulin in lower molecular weight oligomeric conformations, which was further corroborated with ThT and DLS data (Figure 2D, 2E, S3B, and S3C).

IS1 maintains insulin in a thermostable bioactive conformation

To find whether IS1 confers insulin stabilization in physiologically active conformers, we performed an ITT in mice. IS1-treated bovine insulin followed similar glucose-lowering kinetics to that of native insulin during the ITT even after heat-induced fibrillation induction, while fibrillated insulin revealed a marked impairment in glucose-lowering potential (Figure 3A). Next, we developed two independent disease mouse models, streptozotocin-induced type 1 diabetes and high-fat-diet-fed type 2 diabetes. Expectedly, the addition of IS1 significantly restored the glucose-lowering activity of insulin, effects that were comparable with native insulin in both the disease models (Figures 3B and 3C). IS1 also preserves the bioactivity of Actrapid even after 37°C storage for 30 days as depicted by ITT (Figure 3D). For further affirmation, we investigated the induction of prototypical signaling cascade for the IS1-insulin complex. We observed a marked induction of Akt phosphorylation in IS1-treated insulin compared with that of fibrillated insulin both in cultured hepatocytes (Figure S3D) and in the mouse liver (Figure 3E). Insulin-derived amyloidosis is defined as a subcutaneous amyloid mass at the site of insulin injections owing to intrinsic fibrillation of commercial insulin owing to long-term storage. To this end, we carried out amyloidoma formation assay (Figure 3F) where repeated subcutaneous injection of fibrillated insulin forms a mass of extracellular amyloid fibrils in mice.

IS1 has limited cytotoxicity with no membrane permeability

Toward further characterization of IS1 peptide, we checked for its membrane permeability using fluorescein isothiocyanate (FITC)-labeled IS1 in HepG2 cells. FITC fluorescence was observed in the extracellular space even after 24 h of incubation, whereas FITC-SLRP (Jana et al., 2018), a cell-penetrating tetrapeptide, was detected intracellularly (Figure 4A). The spatial distribution (FITC) IS1-insulin complex showed preferential accumulation on the cell membrane suggesting its receptor binding potential (Figure 4B). Cytotoxicity has often been implicated in short peptides even for the cell-impermeable peptides. Both

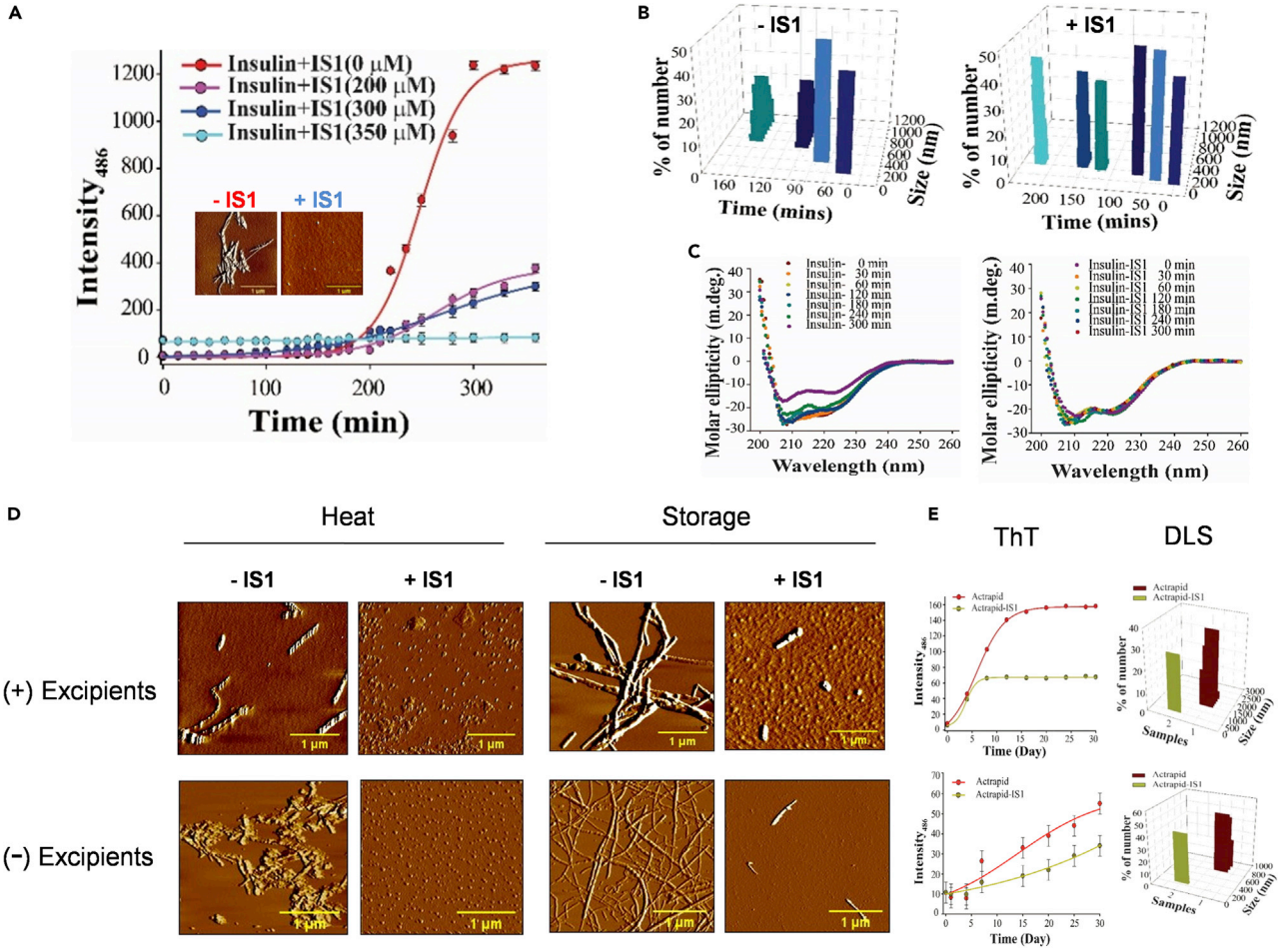

Figure 2. IS1 prevents intrinsic fibrillation of insulin

(A) ThT assay of insulin fibrillation with increasing concentrations of IS1(VVYR). Inset: AFM images of heat-induced fibrillation of insulin in the presence of IS1 (scale bars, 1 μm).

(B) DLS analysis as a function of incubation time of insulin (left panel) and IS1-insulin complex (right panel).

(C) CD spectra of insulin in the absence (left panel) and the presence (right panel) of IS1.

(D) AFM images of heat-induced and storage-induced fibrillation of Actrapid with IS1 in the presence and absence of excipients (scale bars, 1 μm).

(E) ThT and DLS assay for storage-induced fibrillation of Actrapid and Actrapid-IS1 in the presence and absence of commercial excipients. All experiments were performed in triplicates, and values are presented as mean ± SEM.

dose-dependent and time-course cytotoxicity assays showed limited cytotoxicity of IS1 toward HepG2 cells using live-dead and MTT assays (Figures 4C–4E). Consistently, IS1 leads to only ~0.5% hemolysis compared with 1% Triton X-100 (Figure 4F).

Nuclear magnetic resonance spectroscopy reveals the structure and dynamics of IS1 and insulin interaction

For structural characterization and deciphering atomic level interaction of the insulin-IS1 complex, we performed a series of nuclear magnetic resonance (NMR) spectroscopy experiments. One-dimensional STD NMR experiment showed that aromatic protons of tyrosine Y2 (2.6 H), Y3(2.6 H); side chain of arginine R4 QD; and the β-proton of tyrosine Y2 Hβ1 and Y3 Hβ2 interacting with insulin which was also found to be interacting with Actrapid (Figures S4A–S4D). To reveal the atomic-level dynamics of free IS1 and IS1-insulin complex, one-dimensional longitudinal ($R_1 = 1/T_1$) and transverse relaxation ($R_2 = 1/T_2$) experiments were performed. We observed a significant decrease in longitudinal relaxation rate (R_1) for the IS1-insulin complex compared with free IS1 for all amide protons. Similarly, the transverse relaxation rates (R_2) for all the residues of IS1 were increased in the presence of insulin stating spin-spin energy exchange in the

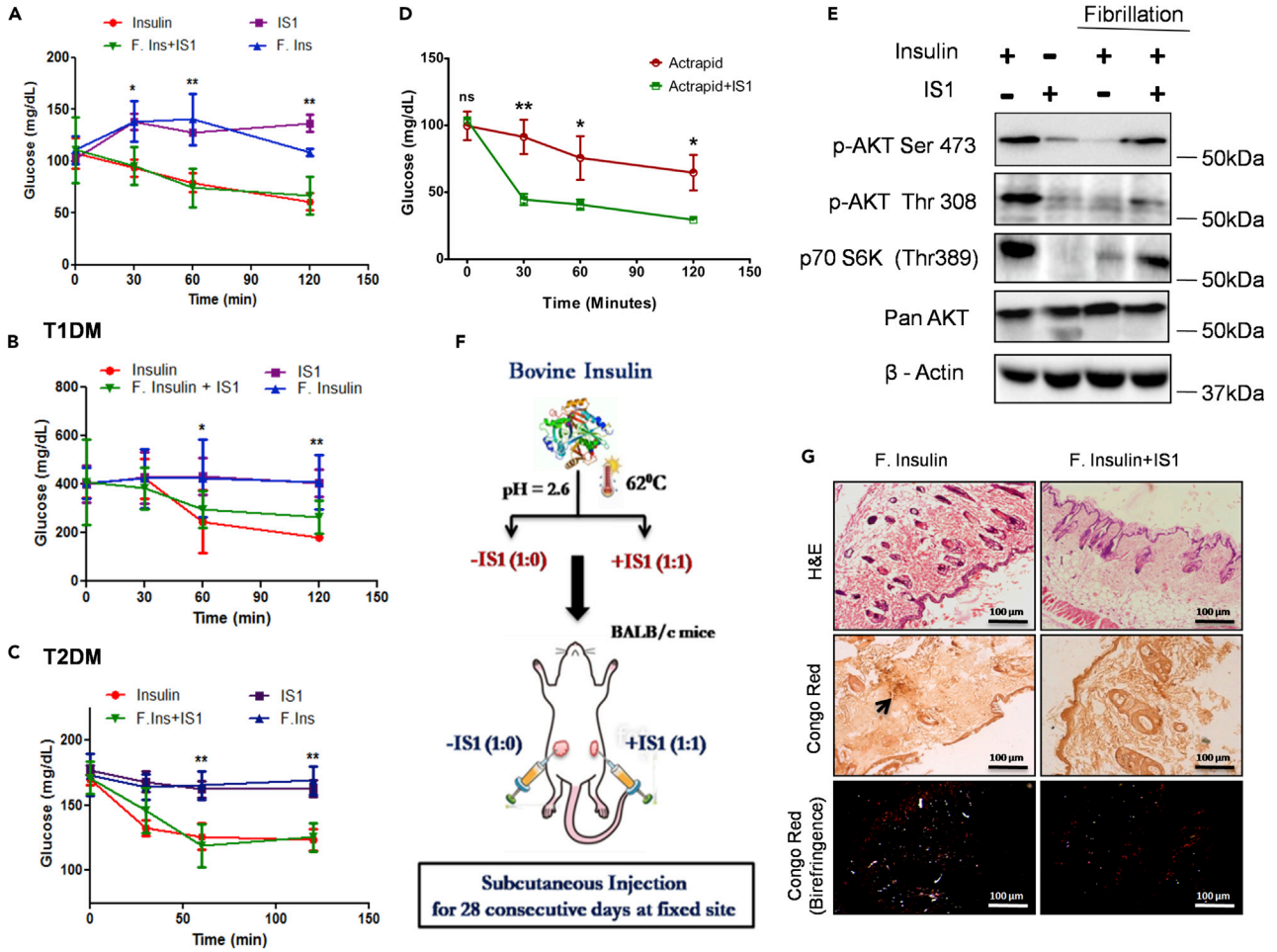

Figure 3. IS1 maintains insulin in a thermostable bioactive conformation

(A–C) ITT of heat-induced fibrillated insulin with IS1 in BALB/c mice (A), preclinical models of type 1 diabetes (B), and type 2 diabetes (C) [n = 5/group].

(D) ITT of storage-induced fibrillated Actrapid in BALB/c mice [n = 5/group].

(E) Western blot of Akt (Ser 473, Thr 308) and p70S6K phosphorylation in BALB/c mice liver. pan AKT and β-actin served as a loading control.

(F) Schematics of generating local amyloidosis in mice by subcutaneous injection of insulin amyloid fibrils.

(G) Visualization of amyloid deposition for both fibrillated insulin (left panel) and fibrillated insulin with IS1 (right panel) in skin biopsies stained with hematoxylin and eosin (H&E) and Congo Red using light and polarized microscopy (scale bars, 100 µm) [n = 3/group]. Values are presented as mean ± SEM. ns, not significant. *p < 0.05, **p < 0.01, ***p < 0.001.

horizontal plane which confirms complexation (Figure S5A). Amide exchange of insulin in presence of IS1 at a varying temperature ranging from 25°C to 65°C showed almost no exchange dictating that IS1 prevents unfolding of monomeric globular insulin (Figure S5B).

The ^{1}H–^{1}H 2-dimensional (2D) NOESY experiment has traced the NOESY contacts [Y2(peptide):Y19(insulin)], [R4(peptide):N24(insulin)], [Y3(peptide):S12(insulin)], [V1(peptide):E17(insulin)], [Y3(peptide):V10(insulin)], thereby identifying the atomic interactions between IS1 and monomeric insulin (Figure 5A). A 3-dimensional (3D) (^{1}H-^{1}H-^{15}N) NOESY-HSQC experiment further confirmed the interaction of terminal R4 of IS1 with ASN24 of the insulin B-chain (Figure 5B).

Based on 2D and 3D NMR spectroscopy, inter-residual NOESY distance restraints were made using a semi-quantitative method keeping the ASN24-R4 contact strong (derived from precision dock analysis in Schrodinger's suite), and the distance-restrained NMR-derived structure calculation of insulin-IS1 complex was performed. From the final 10 restrained MD structures, the insulin-IS1 inter-residual contacts were found and compared with the evolved 3D and 2D NOESY data set (Figure 5C). Molecular dynamics simulation

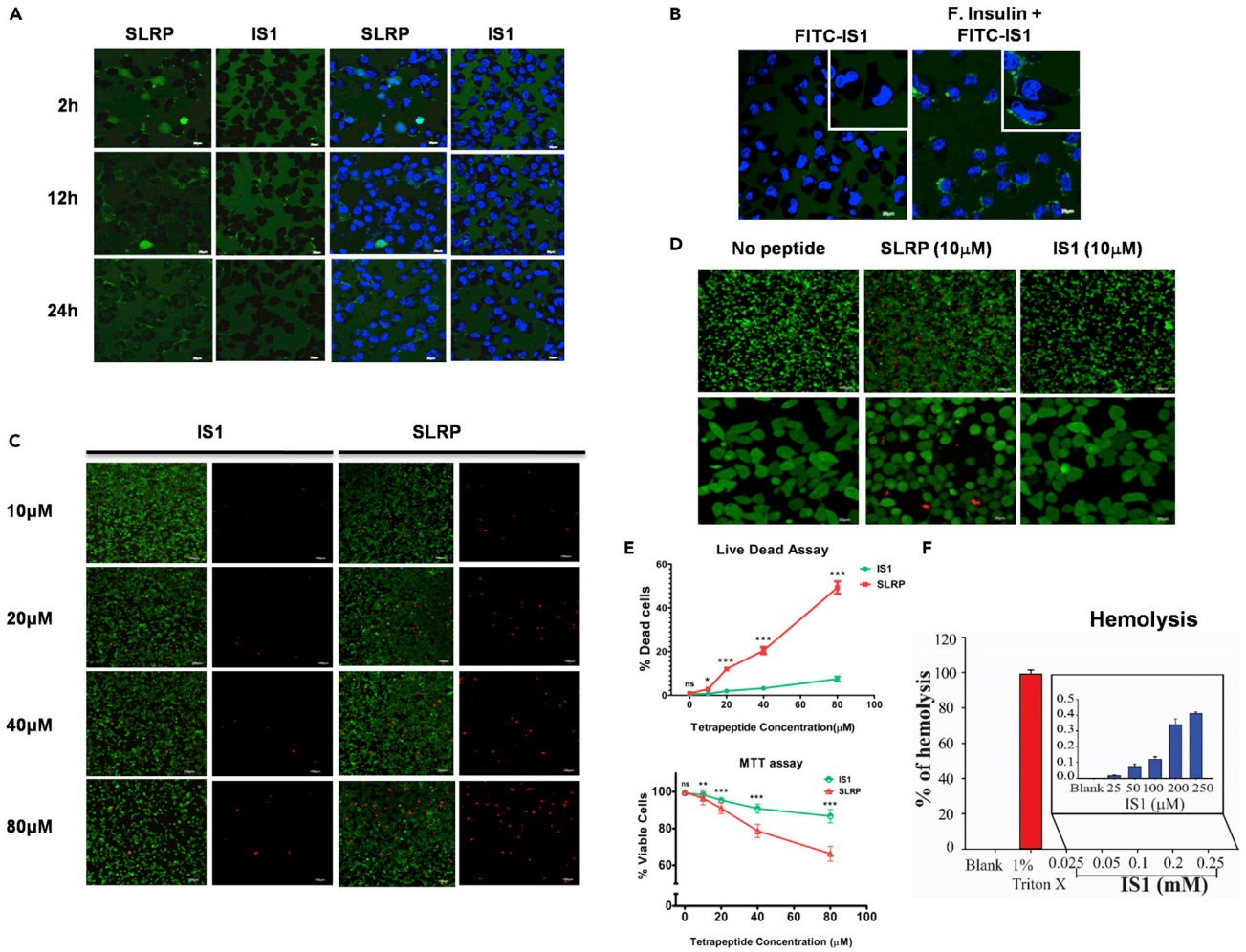

Figure 4. IS1 serves as a potent nontoxic membrane-impermeable stabilizer for insulin

(A) Confocal microscopy images showing time-dependent cell membrane permeability using FITC-tagged tetrapeptide SLRP and IS1 (VYYR), respectively, at 10 μM concentration for 24 h in HepG2 cell line (scale bars, 20 μm).

(B) Representative confocal images showing localization of FITC-IS1 independently and in the presence of native bovine insulin heated at 62°C for 3 h, treated in HepG2 cells (scale bars, 20 μm). Inset represents a 5X digitally magnified image of respective samples (scale bars, 10 μm).

(C) Dose-dependent live/dead cell viability assay showing live cells stained with Calcein-AM (green) and dead cells with EthD-1 (red) treated for 12 h with both SLRP and IS1 in HepG2 cells (scale bars, 100 μm).

(D) Live/Dead cell viability assay of HepG2 cells in the presence of both IS1 and SLRP independently at 10 μM concentration for 24 h in HepG2 cell line (upper panel: scale bars 100 μm; lower panel: scale bars 20 μm).

(E) Top: quantification of percent dead cells at each concentration of respective tetrapeptide IS1 and SLRP treatment. Quantified using threshold and analyze particle function using Fiji (ImageJ) software (5 fields for each concentration of samples). Bottom: MTT assay showing the percent of viable cells at each concentration of respective tetrapeptide IS1 and SLRP treatment.

(F) Hemolytic assay results in negligible hemolysis compared with 1% Triton X-100. Values are presented as mean ± SEM. ns, not significant. *$p < 0.05$, **$p < 0.01$, ***$p < 0.001$.

for free insulin and IS1-insulin complex has revealed the interactions between Y2 (peptide) and E34 (B-chain of insulin), V1 (peptide), and H26 (B-chain of insulin), Y3 (peptide), and Q25. The R4 of V-Y-Y-R forms a triad H-bond network among Val10 (A chain of insulin) and Asn24 (B chain of insulin) (Figure 5D i-v). The adaptive Poisson-Boltzmann surface area (APBS) was calculated for the insulin-IS1 complex. The blue and red surfaces designate positive and negative electronic charge surfaces in APBS, respectively (Figure S5D i-iii).

Previous studies suggested that B-chain N-terminal residues (Phe22-Gly29) of insulin are critical for dimer-dimer interactions that essentially induce R6 hexameric conformation in the presence of Zn+ and phenolic excipients. The exchange of Asn24 for lysine affects monomerhexamer equilibria that allow

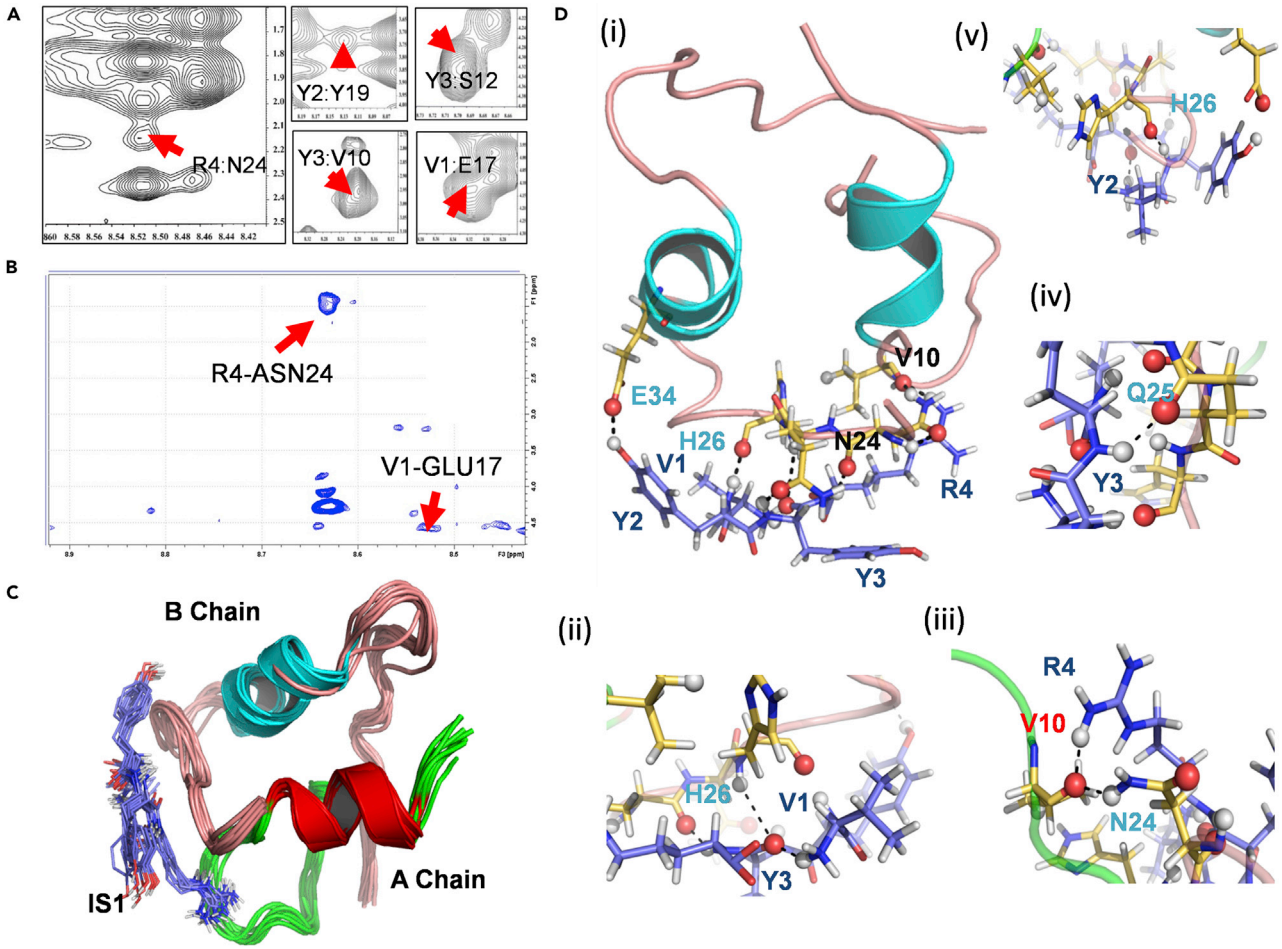

Figure 5. NMR spectroscopy and restrained molecular simulation model of the insulin-IS1 complex

(A) 2D NOESY NMR peak of IS1 interacting with insulin and forming cross-peaks.

(B) 3D 15N-HSQC-NOESY spectrum of insulin in presence of IS1.

(C) The ensemble structure of restrained simulation of insulin-IS1 of the last 10 ps.

(D,i-v) Residue specific atomic interactions depicting a triad hydrogen bond network; molecular simulation showing the interactions between Y2 (peptide) and E34 (B-chain of insulin), V1 (peptide) and H26 (B-chain of insulin), Y3 (peptide) and Q25.

dimerization but predominantly prevent conformational transition toward R6 hexamers, even in the presence of zinc. But, protein engineering studies revealed that the removal or exchange of amino acids at B-chain C-terminus (Tyr47-Thr51) drastically impairs the self-association of the insulin monomers (dimerization). Interestingly, short-acting insulin glulisine bearing mutation at N24 and N50 favors monomeric structure and is less amenable to fibrillation (Becker, 2007; Woods et al., 2012). Moreover, the N-terminal of B chain is necessary for lateral aggregation so that the protofibrils can form fibrils (Jiménez et al., 2002). Atomic traces from NMR and simulation studies of the IS1-insulin complex suggest that the binding of IS1 restricts insulin from having sufficient degrees of freedom to misfold under biophysical perturbations while restricting conformational transitions by forming ^{IS1}(R4)-(V10-N24)^{INS} triad hydrogen bond network.

Dimer stability is crucial for IS1-mediated insulin stabilization

To investigate the mechanism of IS1-mediated insulin stabilization under physicochemical perturbations, size exclusion chromatography was performed for fibrillated human insulin in the presence and absence of IS1, while native insulin serves as a control. A broad peak was observed within the void volume for heat-induced human insulin-depicting heterogeneous populations of large fibrillar aggregates, whereas native insulin elutes at 118.5 mL. Interestingly, heat-induced insulin in the presence of IS1 showed 4 independent

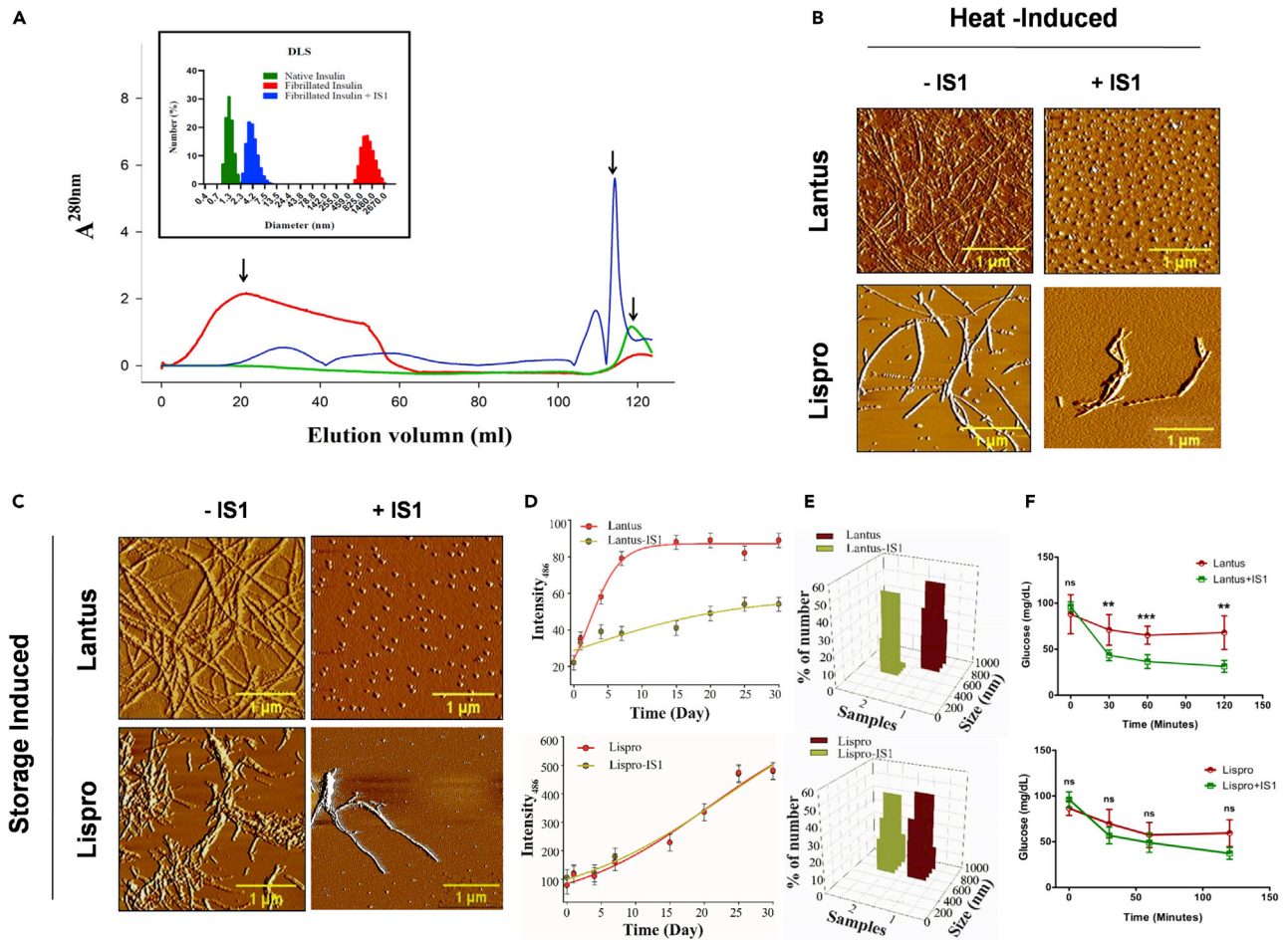

Figure 6. IS1 stabilizes human insulin majorly in dimeric conformation

(A) Size-exclusion profiles of heat-induced recombinant human insulin in the presence and absence of IS1; native human insulin (without heat) serves as a negative control. [Inset] DLS assay were performed for the eluent corresponding to major chromatographic peaks, designated by downsize arrow in size exclusion profiles.

(B) AFM images depicting the heat-induced (62°C, 3 hours) fibrillation of excipients-depleted Lantus and Lispro in the presence and absence of IS1 (scale bars, 1 µm).

(C) AFM images depicting the prolonged storage-induced (37°C, 30 days) fibrillation of excipients-depleted Lantus and Lispro in the presence and absence of IS1 (scale bars, 1 µm).

(D) ThT data for storage-induced fibrillation of excipient-depleted Lantus and Lispro in the presence and absence of IS1.

(E) DLS analysis for storage-induced fibrillation of excipient-depleted Lantus and Lispro in the presence and absence of IS1.

(F) ITT of storage-induced fibrillation of Lantus and lispro (excipient-depleted) in the presence and absence of IS1in BALB/c mice [n = 5 mice/group]. Values are presented as mean ± SEM. *p < 0.05, **p < 0.01, ***p < 0.001.

peaks, while major fraction elutes at 114 mL (Figure 6A). To validate the hydrodynamic properties of all three samples, we have collected the major eluent peaks and performed DLS to reveal the hydrodynamic radius of eluent particles. While native insulin revealed an average hydrodynamic radius of 1.358 nm, heat-induced fibrillated insulin showing a much larger radius ranging from 531 to 3580 nm. Interestingly, fibrillation in the presence of IS1 not only prevents the majority of insulin monomers from getting fibrillated but also the major fraction of eluent particles having the hydrodynamic radius ranging from 3.1 to 4.8 nm (Figure 6A; inset), which overlaps with the dimeric insulin conformers (Pease et al., 2010).

The fibrillation of insulin and its inhibition in the presence of IS1 was next determined by diffusion ordered spectroscopy (DOSY). The larger size (high molecular weight) molecules diffuse at a slower rate than that of smaller size molecules (low molecular weight). The diffusion coefficient obtained from DOSY at 25°C for heated insulin was found to be lower ($\mathbf{D} = 9.4 \times 10^{-5} cm^2 sec^{-1}$) than that of the insulin-IS1 complex

($D = 2.2 \times 10^{-4}$ cm^2sec^{-1}). Besides, the molecular weight of insulin without treatment of IS1 after 4 h incubation at 62°C was approximately 57.0 kDa, supposedly the soluble oligomeric insulin and the insulin-IS1 complex showed much lesser molecular weight approaching 10 kDa representing dimeric insulin conformer (Tables S4A and S4B). These data indicate that the free-insulin undergoes heat-induced oligomerization and conformational switch before its fibrillation, while IS1 protracts insulin oligomerization and hence later aggregation events.

These results prompted us to hypothesize the existence of an IS1-mediated conformation trap between stable hexamer and partially unfolded monomers toward fibrillation. To this end, we have checked the antiamyloid potential of IS1 for two commercially available insulin analogs, Lantus (long-acting) and Lispro (fast-acting). These two analogs were strategically developed majorly to favor hexameric and monomeric conformation, respectively (Figure S6). We removed the existing commercial excipients from both the formulations (Figure S7) for avoiding excipient-induced conformational bias. Interestingly, IS1 significantly protracts fibrillation of Lantus by forming a smaller oligomeric complex in both the storage- and heat-induced condition as depicted by AFM, ThT, and DLS data, whereas it fails to do so for Lispro (Figures 6B–6E). ITT for both Lantus and Lispro in storage-induced fibrillation conditions showed no glucose-lowering potential for Lispro while markedly preserving the physiological role for Lantus (Figure 6F).

We observed a similar trend in the presence of commercial excipients for both Lantus and Lispro (Figures S8 and S9). The one-dimensional STD NMR experiment validated that aromatic protons of tyrosine Y2 Hβ2, Y3Hα, Y3 side chain protons, R4 Hα, and V1 Hα of IS1 interacting with Lantus, while no significantly interacting protons were observed with Lispro (Figure S10A). Even prototypical insulin signaling in HepG2 cells suggests IS1-mediated insulin stabilization leads to biologically active conformers for Actrapid and Lantus but not for Lispro (Figure S10B). Lispro was strategically developed by switching positions of ^{49}Pro-^{50}Lys to ^{49}Lys-^{50}Pro, which greatly reduces its dimerization potential, making it predominantly monomeric fast-acting insulin analog. Hence, dimerization is a crucial determining factor for the antiamyloid potential of IS1, thereby failing to preserve Lispro from physicochemical perturbation-induced fibrillation.

DISCUSSION

The current advocacy of intensive insulin therapy regimens in patients with diabetes is met with several clinical problems – insulin is proamyloidogenic and forms insoluble aggregates resulting in excess insulin requirement; amyloidoma formation at the site of repeated insulin injection; gradual loss of excipients and deposition of fibrils in the catheter system of insulin pumps; and temperature-sensitive insulin fibrillation entails storage and maintenance of cold chain. Even mild agitation of insulin during its storage and transport has been reported to denature the protein through fibrillation, resulting in its inactivation. These issues thereby call for a more stable form of formulations that would cater to the increasing global demand.

Taking cues from the conformation-selective surface exposure of "YYR" motif associated with the β-sheet structure in misfolded prion protein PrP^{Sc}, we discovered a consensus amino acid sequence VXYR as a potent inhibitor for both purified and commercial insulin formulations. Specifically, the endogenous prion sequence VXYR (termed here IS1), a plasma-membrane-impermeable, nontoxic tetrapeptide showed remarkable protraction of insulin fibrillation on heating and during prolonged storage, maintained hypoglycemic effects *in vivo*, and prevented subcutaneous amyloidoma formation. These effects were mediated via direct binding of IS1 to insulin monomer through a triad hydrogen bond network that leads to noncanonical dimer-mediated conformational "trapping" of insulin.

Toward development of insulin formulations with lower amyloidogenicity, newer excipients as well as chemically modified insulin moieties are being reported. Recent studies depicted generation of thermostable insulin by adding polysialic acid and proline-based homopolymer at specific amino acid residues (Ghosh et al., 2020; Kabotso et al., 2020). Aromatic small molecules such as resveratrol and rosmarinic acid were shown to enhance the biophysical stability of native insulin while preserving its physiological activity by stabilizing the hexameric form or preventing dimer dissociation, thereby restricting the thermal unfolding of monomers (Pathak et al., 2020; Zheng and Lazo, 2018). In the present study, we have identified IS1 or VYYR, isosequential to the β-2 strand of human PrP^{C}, as one small endogenous tetrapeptide motif that prevents both heat- and storage-induced insulin fibrillation both

in vitro and *in vivo* and described a noncanonical molecular mechanism for inhibiting insulin fibrillation. Peptide screening assay further highlights the position-specific sequence conservation of IS1 in preserving its antiamyloid potential with a consensus amino acid sequence V-X-Y-R having a potent antiamyloid activity.

Mechanistically, IS1 predominantly binds to the N-terminal of B chain of insulin, forming a triad hydrogen bond network (R4 (peptide)-V10(insulin)-N24(insulin)). Interestingly, short-acting insulin glulisine bearing mutation at N24 and N50 favors monomeric structure and is less amenable to fibrillation (Becker, 2007; Woods et al., 2012; Zhou et al., 2016). Direct interaction of IS1 to N24 may thus confer its conformational stability. The residues from 31 to 41 of B chain form the hydrophobic core in insulin fibril, while residues of 13–18 of A chain are susceptible to conversion from α-helix to beta strands when misfolded. Moreover, the N-terminal of B chain is necessary for lateral aggregation so that the protofibrils can form fibrils (Jiménez et al., 2002). STD NMR deciphered Y2 (2.6 H), Y3 (2.6 H), Y2 (Hβ1), and Y3 (Hβ2) protons of IS1 interact with insulin monomer. Insulin in solution confers bioactive monomer to zinc-coordinated less-active hexameric forms transitioning through intermediated dimeric states. While monomeric forms are more susceptible to fibrillate, hexamers are somewhat immune to fibrillation. DLS data of the size-exclusion chromatography profile suggested that the binding of IS1 to insulin preferentially "trap" insulin in the dimeric conformation (Figure 6A), which not only limits the degrees of freedom to misfold under biophysical perturbations but allows the release of active monomers as needed.

IS1-stabilized insulin showed glucose-lowering ability and signaling potential that were comparable with native insulin. Experiments in type 1 and type 2 diabetes mellitus mice models and different commercially available insulin formulations in the presence and absence of excipients for both heat- and prolonged storage-induced insulin fibrillation further suggests its therapeutic potential. Peptide solubility holds the major concern restricting the potential use in commercial formulations. We find IS1 is highly soluble in citrate phosphate buffer (pH 2.6) up to 10 mM concentration (the maximum concentration that we have checked) and in distilled water. Moreover, the tetrapeptide is soluble in various commercial insulin formulations (Actrapid, pH 7; Lispro, pH 7–7.8; and Lantus, pH 4) both in the presence and absence of variable salts and nonpolar excipients for at least 1 mM concentration. IS1 is cell-impermeable and nontoxic and has previously been shown to be nonimmunogenic (Caughey, 2003; Paramithiotis et al., 2003; Taschuk et al., 2014), further attributing to its future potential as a thermostable insulin stabilizer.

Limitations of the study

The present study has few potential limitations which we believe could create future research opportunities. Although we have generated compelling NMR data for elucidating mechanistic underpinnings of IS1's antiamyloid potential, it still remains incomplete. X-ray crystallography of the IS1-insulin complex would better clarify the molecular mechanism. Moreover, cellular toxicity data are preliminary and further *in vivo* studies including pharmacokinetic and pharmacodynamic profiles would be required for possible future development of therapeutics.

Resource availability

Lead contact

Further information and requests for resources and reagents should be directed to and will be fulfilled by the lead contact: Partha Chakrabarti (Email: pchakrabarti@iicb.res.in).

Materials availability

This study did not generate new unique reagents.

Data and code availability

The accession number of the NMR derived structure is available with IDs i.e. PDB ID 7ELJ, BMRB ID 36417.

SUPPLEMENTAL INFORMATION

Supplemental information can be found online at https://doi.org/10.1016/j.isci.2021.102573.

ACKNOWLEDGMENTS

SC is thankful to the Bose Institute's NMR facility of 700 MHz Bruker. SC thanks Prof. Uday Bandyopadhyay for his generous support and DST, Govt of India for funding. We would also like to thank Dr. Surajit Ghosh for providing FITC-SLRP peptide. We thank T. Muruganandan for his help with AFM experiments at IICB.

SC is thankful to Bose Institute's intramural fund. PC acknowledges intramural funding from CSIR-IICB.

AUTHOR CONTRIBUTIONS

SC initiated the research and designed the prion derived peptide. PC (IICB) and SC (BI) conceived the idea to proceed with peptide screening. Biophysical experiments such as all the fibrillation assays, ITC, DLS, and CD spectroscopy were designed, analyzed by SC, MM, and executed by MM. Some peptides were synthesized by MM. Peptide screening was performed by DD and MM, whereas analyzed by DD, JS, and PC. NMR data acquisition and analysis were performed by MM, NB, JRG and SC. NMR derived structure calculations were performed by NB and SC in AMBER 14.0. Size-exclusion chromatography coupled with DLS experiments were performed by NB and analyzed by NB and SC. All the in-cellulo and *in vivo* assays were performed by DD and analyzed by DD and PC. AFM data execution was performed by DD and analyzed by DD and PC. 3D NMR data execution was performed by JB and analyzed by MM, NB. The manuscript was written by DD, MM, SC, and PC.

DECLARATION OF INTERESTS

There is no conflict of interest.

Received: October 19, 2020
Revised: March 8, 2021
Accepted: May 18, 2021
Published: June 25, 2021

REFERENCES

Amselgruber, W.M., Büttnerbüttner, A.M., Schlegel, A.T., Schweiger, M., and Pfaff, A.E. (2006). The normal cellular prion protein (PrPc) is strongly expressed in bovine endocrine pancreas. Histochem. Cell Biol. *125*, 441–448.

Armiento, V., Hille, K., Naltsas, D., Lin, J.S., Barron, A.E., and Kapurniotu, A. (2020). The human host-defense peptide cathelicidin LL-37 is a nanomolar inhibitor of amyloid self-assembly of islet amyloid polypeptide (IAPP). Angew. Chem. Int. Ed. *59*, 12837–12841.

Ashok, A., and Singh, N. (2018). Prion protein modulates glucose homeostasis by altering intracellular iron. OPEN *8*, 6556.

Banerjee, V., Kar, R.K., Datta, A., Parthasarathi, K., Chatterjee, S., Das, K.P., and Bhunia, A. (2013). Use of a small peptide fragment as an inhibitor of insulin fibrillation process: a study by high and low resolution spectroscopy. PLoS One *8*, e72318.

Baram, M., Gilead, S., Gazit, E., and Miller, Y. (2018). Mechanistic perspective and functional activity of insulin in amylin aggregation. Chem. Sci. *9*, 4244–4252.

Becker, R.H.A. (2007). Insulin glulisine complementing basal insulins: a review of structure and activity. Diabetes Technol. Ther. *9*, 109–121.

Caughey, B. (2003). Probing for prions: recognizing misfolded PrP. Nat. Med. *9*, 819–820.

Das, S., and Bhattacharyya, D. (2017). Destabilization of human insulin fibrils by peptides of fruit bromelain derived from Ananas comosus (pineapple). J. Cell. Biochem. *118*, 4881–4896.

Frankær, C.G., Sønderby, P., Bang, M.B., Mateiu, R.V., Groenning, M., Bukrinski, J., and Harris, P. (2017). Insulin fibrillation: the influence and coordination of Zn 2+. J. Struct. Biol. *199*, 27–38.

Ghosh, P., Bera, A., Ghosh, A., Bhadury, P., and De, P. (2020). Side-chain proline-based polymers as effective inhibitors for in vitro aggregation of insulin*3*, 8th (ACS Applied Bio Materials), pp. 5407–5419.

Gong, H., He, Z., Peng, A., Zhang, X., Cheng, B., Sun, Y., Zheng, L., and Huang, K. (2014). Effects of several quinones on insulin aggregation. Sci. Rep. *4*, 1–8.

Han, X., Park, J., Wu, W., Malagon, A., Wang, L., Vargas, E., Wikramanayake, A., Houk, K.N., and Leblanc, R.M. (2017). A resorcinarene for inhibition of Aβ fibrillation. Chem. Sci. *8*, 2003–2009.

Heller, S., Kozlovski, P., and Kurtzhals, P. (2007). Insulin's 85th anniversary-An enduring medical miracle. Diabetes Res. Clin. Pract. *78*, 149–158.

Hua, Q.X., and Weiss, M.A. (2004). Mechanism of insulin fibrillation: the structure of insulin under amyloidogenic conditions resembles a protein-folding intermediate. J. Biol. Chem. *279*, 21449–21460.

Ivanova, M.I., Sievers, S.A., Sawaya, M.R., Wall, J.S., and Eisenberg, D. (2009). Molecular basis for insulin fibril assembly. Proc. Natl. Acad. Sci. U. S. A. *106*, 18990–18995.

Jana, B., Mondal, P., Saha, A., Adak, A., Das, G., Mohapatra, S., Kurkute, P., and Ghosh, S. (2018). Designed tetrapeptide interacts with tubulin and microtubule. Langmuir *34*, 1123–1132.

Jiménez, J.L., Nettleton, E.J., Bouchard, M., Robinson, C.V., Dobson, C.M., and Saibil, H.R. (2002). The protofilament structure of insulin amyloid fibrils. Proc. Natl. Acad. Sci. U. S. A. *99*, 9196–9201.

Julien, O., Chatterjee, S., Thiessen, A., Graether, S.P., and Sykes, B.D. (2009). Differential stability of the bovine prion protein upon urea unfolding. Protein Sci. *18*, 2172–2182.

Kabotso, D.E.K., Smiley, D., Mayer, J.P., Gelfanov, V.M., Perez-Tilve, D., Dimarchi, R.D., Pohl, N.L.B., and Liu, F. (2020). Addition of sialic acid to insulin confers superior physical properties and bioequivalence. Cite This J. Med. Chem. *63*, 6143.

Kachooei, E., Moosavi-Movahedi, A.A., Khodagholi, F., Mozaffarian, F., Sadeghi, P., Hadi-Alijanvand, H., Ghasemi, A., Saboury, A.A., Farhadi, M., and Sheibani, N. (2014). Inhibition study on insulin fibrillation and cytotoxicity by paclitaxel. J. Biochem. *155*, 361–373.

Lee, H.H., Choi, T.S., Lee, S.J.C., Lee, J.W., Park, J., Ko, Y.H., Kim, W.J., Kim, K., and Kim, H.I. (2014). Supramolecular inhibition of amyloid

fibrillation by cucurbit[7]uril. Angew. Chemie - Int. Ed. *53*, 7461–7465.

Mishra, N.K., Joshi, K.B., and Verma, S. (2013). Inhibition of human and bovine insulin fibril formation by designed peptide conjugates. Mol. Pharm. *10*, 3903–3912.

Moroder, L., and Musiol, H.J. (2017). Insulin—from its discovery to the industrial synthesis of modern insulin analogues. Angew. Chem. - Int. Ed. *56*, 10656–10669.

Neddenriep, B., Calciano, A., Conti, D., Sauve, E., Paterson, M., Bruno, E., and Moffet, A.D. (2012). Short peptides as inhibitors of amyloid aggregation. Open Biotechnol. J. *5*, 39–46.

Nilsson, M.R. (2016). Insulin amyloid at injection sites of patients with diabetes. Amyloid *23*, 139–147.

Owens, D.R., Zinman, B., and Bolli, G.B. (2001). Insulins today and beyond. Lancet *358*, 739–746.

Paramithiotis, E., Pinard, M., Lawton, T., LaBoissiere, S., Leathers, V.L., Zou, W.Q., Estey, L.A., Lamontagne, J., Lehto, M.T., Kondejewski, L.H., et al. (2003). A prion protein epitope selective for the pathologically misfolded conformation. Nat. Med. *9*, 893–899.

Patel, P., Parmar, K., and Das, M. (2018). Inhibition of insulin amyloid fibrillation by Morin hydrate. Int. J. Biol. Macromol. *108*, 225–239.

Pathak, B.K., Das, D., Bhakta, S., Chakrabarti, P., and Sengupta, J. (2020). Resveratrol as a nontoxic excipient stabilizes insulin in a bioactive hexameric form. J. Comput. Aided. Mol. Des. *34*, 915–927.

Pease, L.F., Iii, Sorci, M., Guha, S., Tsai, D.-H., Zachariah, M.R., Tarlov, M.J., and Belfort, G. (2010). Probing the nucleus model for oligomer formation during insulin amyloid fibrillogenesis. Biophys J. *99*, 3979–3985.

Ratha, B.N., Ghosh, A., Brender, J.R., Gayen, N., Ilyas, H., Neeraja, C., Das, K.P., Mandal, A.K., and Bhunia, A. (2016). Inhibition of insulin amyloid fibrillation by a novel amphipathic heptapeptide: mechanistic details studied by spectroscopy in combination with microscopy. J. Biol. Chem. *291*, 23545–23556.

Saithong, T., Thilavech, T., and Adisakwattana, S. (2018). Cyanidin-3-rutinoside reduces insulin fibrillation and attenuates insulin fibrils-induced oxidative hemolysis of human erythrocytes. Int. J. Biol. Macromol. *113*, 259–268.

Seidler, P.M., Boyer, D.R., Rodriguez, J.A., Sawaya, M.R., Cascio, D., Murray, K., Gonen, T., and Eisenberg, D.S. (2018). Structure-based inhibitors of tau aggregation. Nat. Chem. *10*, 170–176.

Taschuk, R., Marciniuk, K., Määttänen, P., Madampage, C., Hedlin, P., Potter, A., Lee, J., Cashman, N.R., Griebel, P., and Napper, S. (2014). Safety, specificity and immunogenicity of a PrPSc-specific prion vaccine based on the YYR disease specific epitope. Prion *8*, 51–59.

Teska, B.M., Alarcõn, J., Pettis, R.J., Randolph, T.W., and Carpenter, J.F. (2014). Effects of phenol and meta-cresol depletion on insulin analog stability at physiological temperature. J. Pharm. Sci. *103*, 2255–2267.

Wallin, C., Hiruma, Y., Wärmländer, S.K.T.S., Huvent, I., Jarvet, J., Abrahams, J.P., Gräslund, A., Lippens, G., and Luo, J. (2018). The neuronal tau protein blocks in vitro fibrillation of the amyloid-β (Aβ) peptide at the oligomeric stage. J. Am. Chem. Soc. *140*, 8138–8146.

Wang, J.B., Wang, Y.M., and Zeng, C.M. (2011). Quercetin inhibits amyloid fibrillation of bovine insulin and destabilizes preformed fibrils. Biochem. Biophys. Res. Commun. *415*, 675–679.

Weber, C., Kammerer, D., Streit, B., and Licht, A.H. (2015). Phenolic excipients of insulin formulations induce cell death, pro-inflammatory signaling and MCP-1 release. Toxicol. Rep. *2*, 194–202.

Woods, R.J., Alarcoń, J., McVey, E., and Pettis, R.J. (2012). Intrinsic fibrillation of fast-acting insulin analogs. J. Diabetes Sci. Technol. *6*, 265–276.

Wu, L.C. (2019). Regulatory Considerations for Peptide Therapeutics. Peptide Therapeutics: Strategy and Tactics for Chemistry, Manufacturing, and Controls (Royal Society of Chemistry), pp. 1–30.

Xiong, X., Blakely, A., Karra, P., Vandenberg, M.A., Ghabash, G., Whitby, F., Zhang, Y.W., Webber, M.J., Holland, W.L., Hill, C.P., and Chou, D.H.C. (2019). Novel four-disulfide insulin analog with high aggregation stability and potency. Chem. Sci. *11*, 195–200.

Yumlu, S., Barany, R., Eriksson, M., and Röcken, C. (2009). Localized insulin-derived amyloidosis in patients with diabetes mellitus: a case report. Hum. Pathol. *40*, 1655–1660.

Zaykov, A.N., Mayer, J.P., and Dimarchi, R.D. (2016). Pursuit of a perfect insulin. Nat. Rev. Drug Discov. *15*, 425–439.

Zheng, Q., and Lazo, N.D. (2018). Mechanistic studies of the inhibition of insulin fibril formation by rosmarinic acid. J. Phys. Chem. B *122*, 2323–2331.

Zhou, C., Qi, W., Lewis, E.N., and Carpenter, J.F. (2016). Characterization of sizes of aggregates of insulin analogs and the conformations of the constituent protein molecules: a concomitant dynamic light scattering and Raman spectroscopy study. J. Pharm. Sci. *105*, 551–558.